12-1-1995

Effect of Disorder on Synchronization in Prototype 2-Dimensional Josephson Arrays

Adam S. Landsberg
Claremont McKenna College; Pitzer College; Scripps College

Yuri Braiman

Kurt Wiesenfeld
Georgia Institute of Technology

Effect of disorder on synchronization in prototype two-dimensional Josephson arrays

A. S. Landsberg, Y. Braiman, and K. Wiesenfeld
School of Physics, Georgia Institute of Technology, Atlanta, Georgia 30332
(Received 7 July 1995)

We study the effects of quenched disorder on the dynamics of two-dimensional arrays of overdamped Josephson junctions. Disorder in both the junction critical currents and resistances is considered. Analytical results for small arrays are used to identify a physical mechanism which promotes frequency locking across each row of the array, and to show that no such locking mechanism exists between rows. The intrarow locking mechanism is surprisingly strong, so that a row can tolerate large amounts of disorder before frequency locking is destroyed.

I. INTRODUCTION

Arrays of coupled Josephson junctions have garnered considerable attention in recent years. Their appeal stems both from their potential for device applications,[1,2] and from their theoretical interest as nonlinear, many-degree-of-freedom systems which display some remarkable dynamical features.[3–8] To date, much emphasis has been placed on arrays in which all the junctions are identical. This assumption not only affords some degree of conceptual simplicity to the problem, but is motivated by practical design considerations as well: by combining a large number of identical junctions in an array, collective oscillations of the system become possible, substantially boosting the total output power. This state of perfectly coherent oscillations in a uniform array is known as the "in-phase" state.

Of course, in actual arrays junction uniformity is good but not perfect: present fabrication techniques allow variations in the individual junction characteristics on the order of 1%.[9] While such small variations might seem unimportant, recent discoveries have shown that the dynamical equations describing identical junction arrays are quite special: they possess certain highly degenerate structures[7,8] which are not expected to persist once nonuniformities are introduced. For instance, for the type of Josephson array of interest here, the synchronized in-phase state has a high degree of neutral stability.[3,10] Neutral stability is so structurally delicate that, on general theoretical grounds, one expects that *any* small change could fundamentally alter the long-term dynamics. Thus the presence of even small levels of disorder can have important physical implications.

This paper is devoted to understanding the effects of disorder on the synchronization properties of dc-biased, two-dimensional arrays of overdamped Josephson junctions. Allowing variations in junction parameters is a severe theoretical complication: as such, previous investigations of disordered two-dimensional (2D) arrays have been largely numerical.[11–13] Our approach is to analytically study very small arrays, which nevertheless capture the important features of a general $N\times M$ array. We confine our attention to the case of zero magnetic field and no external load. We are able to identify two fundamental physical mechanisms induced by the disorder, and to calculate analytically their effect on the system dynamics. Some of our results can be generalized to the full $N\times M$ case. By combining the analytic results for small arrays with numerical simulations of larger arrays, we are able to construct a fair understanding of the effects of disorder on these 2D arrays.

One of the questions we study concerns the relative dynamical importance of critical current disorder and shunt resistance disorder. We find that the sheer magnitude of the parameter variations does not determine their relative importance: even if the variations in the critical currents are significantly larger than those in the resistances, both can have equally significant dynamical consequences in certain parameter regimes.

This paper is organized as follows. In Sec. II we review the basic behavior of the uniform array model, and describe how disorder is introduced into the system. We find that the dynamical effects of disorder divide naturally into two classes: these are described and analyzed in Secs. III and IV, respectively. Finally, in Sec. V we collect and discuss our main conclusions and compare them with simulations of larger 2D arrays.

II. MODEL EQUATIONS AND THE IN-PHASE STATE

A. The idealized case

We begin by considering a uniform, two-dimensional Josephson junction array, where each junction is described by the resistively shunted junction (RSJ) model,[2] with critical current I_c and resistance r. The governing equation for a single junction is

$$\frac{\hbar}{2er}\dot{\phi}+I_c\sin(\phi)=I, \tag{1}$$

where ϕ denotes the phase difference of the wave function across the superconductor junction, $I=I(t)$ is the total current passing through the junction, and the overdot denotes differentiation with respect to time. The two terms on the left-hand side of (1) represent the regular and supercurrents through the junction, respectively. For fixed dc current I, the junction will overturn [i.e., the time average $\langle\dot{\phi}(t)\rangle\neq 0$] pro-

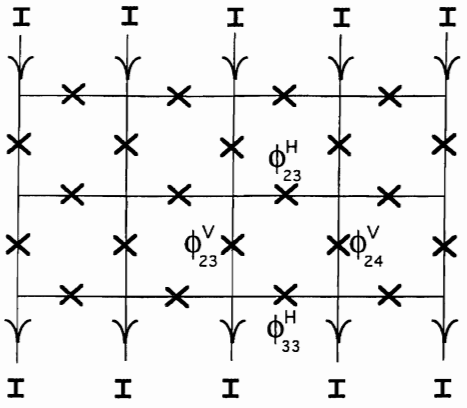

FIG. 1. Josephson junction array. The horizontal junctions are characterized by ϕ^H_{ij}, which measures the phase difference across the jth and $(j+1)$th superconducting lattice sites within row i, and the vertical junctions by ϕ^V_{ij}, measuring the phase difference across the ith and $(i+1)$th sites in column j. Bias current I is injected uniformly along the top row and removed uniformly along the bottom. I^H_{ij} and I^V_{ij} represent the induced currents passing through the horizontal and vertical junctions, respectively.

vided $|I|>I_c$. For the two-dimensional array consisting of $N\times M$ superconducting lattice sites shown in Fig. 1, the equations become

$$\frac{\hbar}{2er}\dot{\phi}^H_{ij}+I_c\sin(\phi^H_{ij})=I^H_{ij},$$
$$i=1,\ldots,N,\quad j=1,\ldots,M-1, \tag{2a}$$

$$\frac{\hbar}{2er}\dot{\phi}^V_{ij}+I_c\sin(\phi^V_{ij})=I^V_{ij},$$
$$i=1,\ldots,N-1,\quad j=1,\ldots,M. \tag{2b}$$

Here, ij labels the superconducting lattice sites, and ϕ^H_{ij} denotes the phase difference of the horizontal junction between the jth and $(j+1)$th lattice sites in row i, and ϕ^V_{ij} the phase difference of the vertical junction between the ith and $(i+1)$th sites within a given column j. The currents passing through the horizontal and vertical junctions are I^H_{ij} and I^V_{ij}, respectively. We have assumed that the array is lumped, which is valid if the physical size of the array is much less than the emission wavelength.

Owing to our choice of the junction phase differences as variables, the above equations are underdetermined. Additional constraints come from the requirement that the sum of the phase differences around any closed path in the lattice must vanish (we will consider only the case of zero magnetic field), along with current conservation and boundary conditions. For the array depicted in Fig. 1, this first constraint takes the form

$$\phi^H_{ij}+\phi^V_{i,j+1}-\phi^H_{i+1,j}-\phi^V_{ij}=0. \tag{3}$$

(Here, i runs from 1 to $N-1$, and j from 1 to $M-1$.) For boundary conditions we assume a constant current I is supplied at each superconducting site along the top row of the array, and removed at each site along the bottom row. This is a common configuration in experiments.[14,9] Since the net current into a given superconducting site is $I^H_{ij}-I^H_{i,j-1}+I^V_{ij}-I^V_{i-1,j}$, current conservations implies

$$I^H_{ij}-I^H_{i,j-1}+I^V_{ij}-I^V_{i-1,j}=\begin{cases} I, & i=1 \\ -I, & i=N \\ 0 & \text{otherwise.}\end{cases} \tag{4}$$

[This constraint relation must be interpreted appropriately at the edges of the array: for $i=1$, $i=N$, $j=1$, or $j=M$, any current in (4) with an index of zero should be neglected.] Together, the constraints (3) and (4) imply that of the $2NM-N-M$ phase differences in (2a) and (2b) only $NM-1$ are independent. This is as it should be, since alternatively we could follow the phases of the NM superconducting islands, which are independent up to an overall (global) phase shift.

B. Neutral stability of the in-phase solution and disorder

The identical-element array admits an in-phase solution, in which all vertical junctions oscillate coherently $[\phi^V_{ij}\equiv\phi^{\rm in}(t)]$, while the horizontal junctions remain inactive $(\phi^H_{ij}=0)$; see Fig. 2. This synchronized state is of particular interest for design applications, and exists if the bias current exceeds I_c, so that the vertical junctions overturn. It has been shown, however, that the in-phase state is neutrally stable with respect to changes in the initial conditions:[3] if the system is perturbed from the in-phase solution, then all variations within a given row damp out $(\phi^H_{ij}\to 0$, $\phi^V_{ij}-\phi^V_{ij'}\to 0)$, but differences between rows do not $(\lim_{t\to\infty}\phi^V_{ij}-\phi^V_{i'j}\neq 0)$. These $N-2$ nondecaying phase differences correspond to neutrally stable directions in phase space. This result follows directly from Floquet theory and remains essentially unchanged even if a parasitic capacitance and inductance is included with each junction.[3,10] Note that the horizontal and vertical junctions play fundamentally distinct roles, and that there is also a dynamical distinction between vertical junctions lying in different rows. This natural division will be exploited later when disorder is introduced.

The emergence of neutral stability can also be understood in a somewhat different manner. Suppose the system is initially in the in-phase state. Now imagine time-advancing all vertical oscillators within a given row (α) by some amount, while holding those in the other rows fixed, i.e., $\phi^V_{\alpha j}(t)\to\phi^{\rm in}(t+\triangle t)$ for all j. Then this new state, $[\phi^H_{ij}=0$, $\phi^V_{i\neq\alpha,j}=\phi^{\rm in}(t)$, $\phi^V_{\alpha,j}=\phi^{\rm in}(t+\triangle t)]$, is itself a valid solution to the dynamical equations (2a) and (2b), as a quick inspection reveals. Hence, the in-phase state belongs to an $(N-1)$-parameter family of phase-locked solutions, with family members related by temporal phase shifts.

Neutral stability of the in-phase state is not simply a mathematical curiosity; rather, it has important physical implications: any modification to the idealized model system (2a) and (2b) — *even an arbitrarily small one* — is potentially capable of stabilizing or destabilizing a neutrally stable

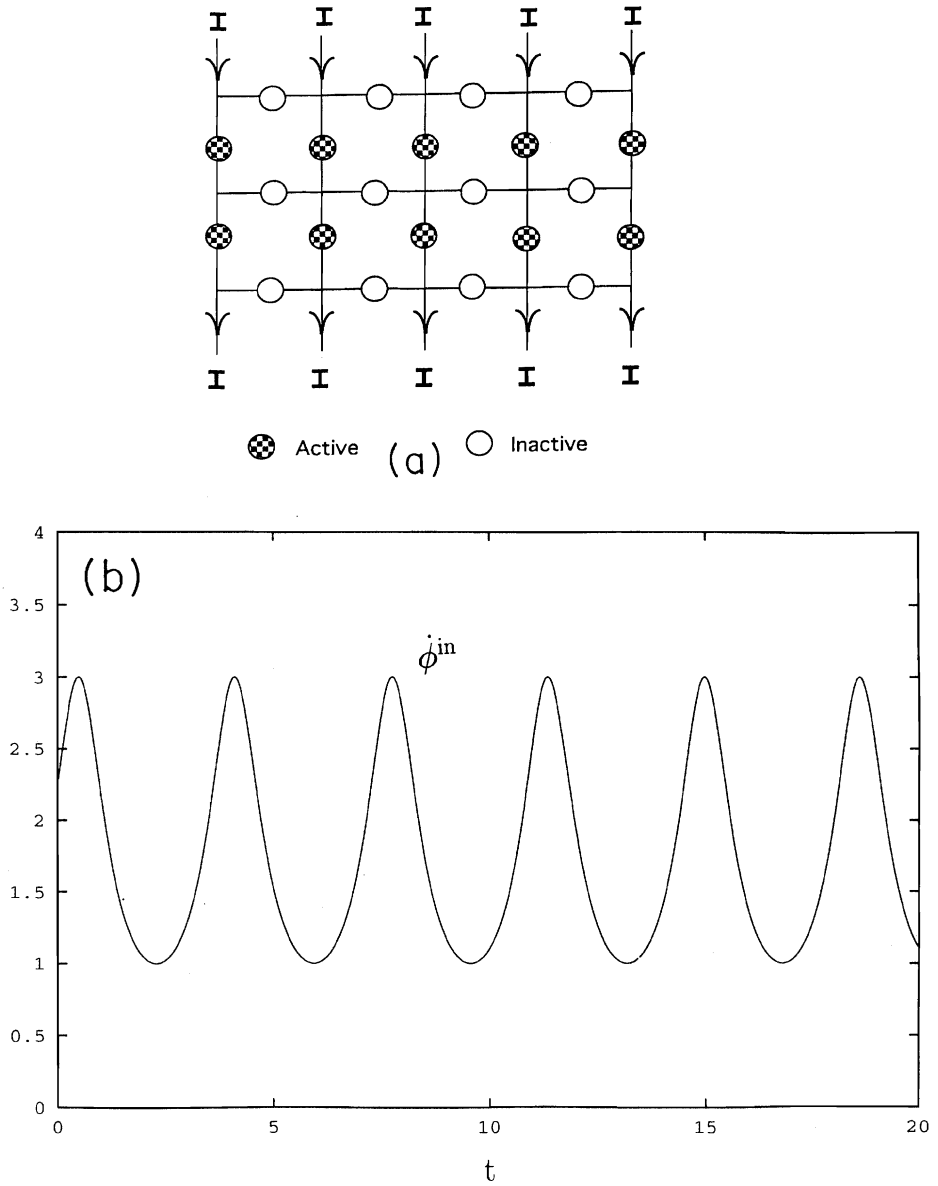

FIG. 2. In-phase state of identical-junction array. (a) shows the direction of current flow, with all horizontal junctions inactive and all vertical junctions having the same functional waveform $\phi^{in}(t)$; (b) representative time series for $\dot{\phi}^{in}(t)$.

state. This point has been demonstrated in the past by considering the effects of external loads,[3,10,11] or alternatively the effect on bare arrays of a small imposed magnetic field perpendicular to the circuit plane.[15,16] Our goal in this paper is to explore an alternative situation: we consider the bare array (no load and no magnetic field) but allow the individual junctions to be slightly nonidentical. It is not clear *a priori* whether any synchronized behavior analogous to the coherent in-phase state is even possible in this case.

From (2a) and (2b), it is clear that disorder (i.e., a spread in the junction parameters) can enter the system through variations in both the critical currents and the resistances of the junctions. (We do not consider here any capacitances or inductances in the junctions.) Hence we replace I_c, r in 2(a) and (2b) by $I_{c_{ij}}^{H,V}$, and $r_{ij}^{H,V}$, respectively. A few crude observations can be made regarding the relative sizes of these two types of imperfections. First, since the critical currents depend exponentially on the gap spacing s between adjacent superconducting sites, while the resistances depend only linearly on s, deviations in the gap spacings will lead to relatively large fractional variations in the critical currents $\{I_{c_{ij}}^{H,V}\}$ compared to the variations in the resistances $\{r_{ij}^{H,V}\}$. This is the origin of the common view that variations in the critical current are in general more important than those in the resistances. On the other hand, since both quantities depend on the area of the superconducting junctions, any variation in this area will lead to comparable-sized fractional variations in the critical currents and resistances. However, we emphasize that both these observations merely relate to the relative sizes of the fractional variations in the two quantities — they say nothing regarding their relative importance in terms of their dynamical effects on the system. In fact, we will show that in certain circumstances (i.e., for high bias currents), even if the variations in the critical currents are

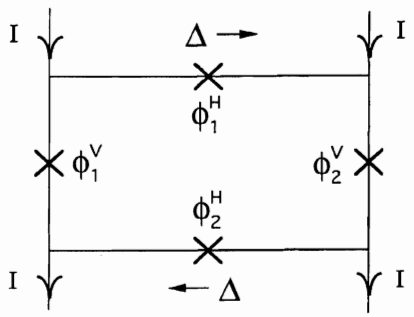

FIG. 3. The plaquette. The phase differences across the vertical and horizontal junctions are denoted by ϕ_1^V, ϕ_2^V and ϕ_1^H, ϕ_2^H, respectively. Current I is imposed at the top and removed at the bottom; $\triangle$ is the induced current shunted across the horizontal junctions.

significantly larger than those in the resistances, both can have equally important dynamical consequences.

Our analysis will be divided into two parts: we first consider the effects of disorder on synchronization within a given row of the system, and then examine synchronization effects between rows. This natural division is motivated by our previous observation that the vertical junctions in different rows play fundamentally distinct roles in the coherent oscillations of the ideal, identical-junction array (2a) and (2b). We proceed by studying analytically the smallest 2D arrays which capture the principle mechanisms at work in the (i) intrarow dynamics and then (ii) interrow dynamics. We find that some of our results readily generalize to arbitrary $N \times M$ arrays.

III. DYNAMICS WITHIN A ROW

Recall that in the ideal (identical-junction) array, perturbations of the in-phase state within each row are exponentially damped, leading to uniform in-phase oscillations across each row. Although the perfect in-phase solution no longer exists once disorder is introduced, we expect that some type of in-row locking mechanism may persist. With this in mind, we consider the simplest array capable of describing dynamical coupling between oscillators within a given row. This 2×2 array (the so-called plaquette) is depicted in Fig. 3. From (2a) and (2b) together with constraint (4), the dynamical equations for the plaquette take the form

$$\frac{\hbar}{2er_1^H}\dot{\phi}_1^H + I_{c_1}^H \sin(\phi_1^H) = \triangle, \tag{5a}$$

$$\frac{\hbar}{2er_2^H}\dot{\phi}_2^H + I_{c_2}^H \sin(\phi_2^H) = -\triangle, \tag{5b}$$

$$\frac{\hbar}{2er_1^V}\dot{\phi}_1^V + I_{c_1}^V \sin(\phi_1^V) = I - \triangle, \tag{5c}$$

$$\frac{\hbar}{2er_2^V}\dot{\phi}_2^V + I_{c_2}^V \sin(\phi_2^V) = I + \triangle, \tag{5d}$$

where we have defined $\triangle \equiv I_1^H = -I_2^H$ and allowed the junctions to be nonidentical. The remaining constraint relation (3) becomes

$$\phi_1^H + \phi_2^V - \phi_2^H - \phi_1^V = 0, \tag{6}$$

and can be used to eliminate one of the four phase variables in Eqs. (5a)–(5d), and permits $\triangle$ to be reexpressed in terms of the remaining three phases.

A. Locking in the plaquette: Physical argument

We now construct a simple physical argument for how disorder affects the dynamics of the plaquette; a more rigorous derivation is presented in the next section. Consider first the case of identical junctions. In the ideal in-phase state (with $I > I_c$), the vertical junctions are overturning and phase locked ($\phi_1^V = \phi_2^V$), the horizontal junctions are inactive ($\phi_1^H = \phi_2^H = 0$), and the transverse shunt current $\triangle$ is zero. If weak disorder is now introduced, we expect that the vertical junctions will no longer be phase locked, but may remain frequency locked if just the right amount of supercurrent is spontaneously induced to compensate for the disorder. This could be accomplished by means of nonzero shunt currents passing across the horizontal junctions, which are now active due to the disorder but do not overturn (i.e., $\dot{\phi}_j^H \neq 0$ but $\langle \dot{\phi}_j^H \rangle = 0$). We can estimate the amount of shunt current required for locking as follows. For simplicity, assume that all junctions have the same resistance r, so that the disorder in the system is due solely to variations in the critical currents. The shunt current $\triangle$ will oscillate about some mean $\langle \triangle \rangle$. As a first approximation we neglect these oscillations and replace $\triangle$ in (5a)–(5d) by its time average. The system may now be integrated directly, and from (5c) and (5d) we find that the vertical junctions ϕ_1^V and ϕ_2^V overturn with an average frequency of $\sqrt{(I - \langle \triangle \rangle)^2 - (I_{c_1}^V)^2}$, and $\sqrt{(I + \langle \triangle \rangle)^2 - (I_{c_2}^V)^2}$, respectively. Equating these two frequencies and solving for $\langle \triangle \rangle$ yields

$$\langle \triangle \rangle = \frac{(I_{c_2}^V)^2 - (I_{c_1}^V)^2}{4I}. \tag{7}$$

This simple picture also allows us to estimate the maximum amount of disorder the system can tolerate before frequency locking breaks down. As the deviation in the critical currents is increased, the system will remain locked provided there is sufficient supercurrent to be shunted across the horizontal junctions. At a certain point, the required shunt current (7) will exceed the maximum supercurrent which can be passed by the horizontal junctions, $(I_{c_1}^H, I_{c_2}^H)$. These junctions will thus begin to overturn, regular current will flow, and the locking between the vertical junctions will be destroyed. This transition between the locked and unlocked states occurs when $\min(I_{c_1}^H, I_{c_2}^H) = |\langle \triangle \rangle|$. From (7), we therefore expect locking to be possible provided

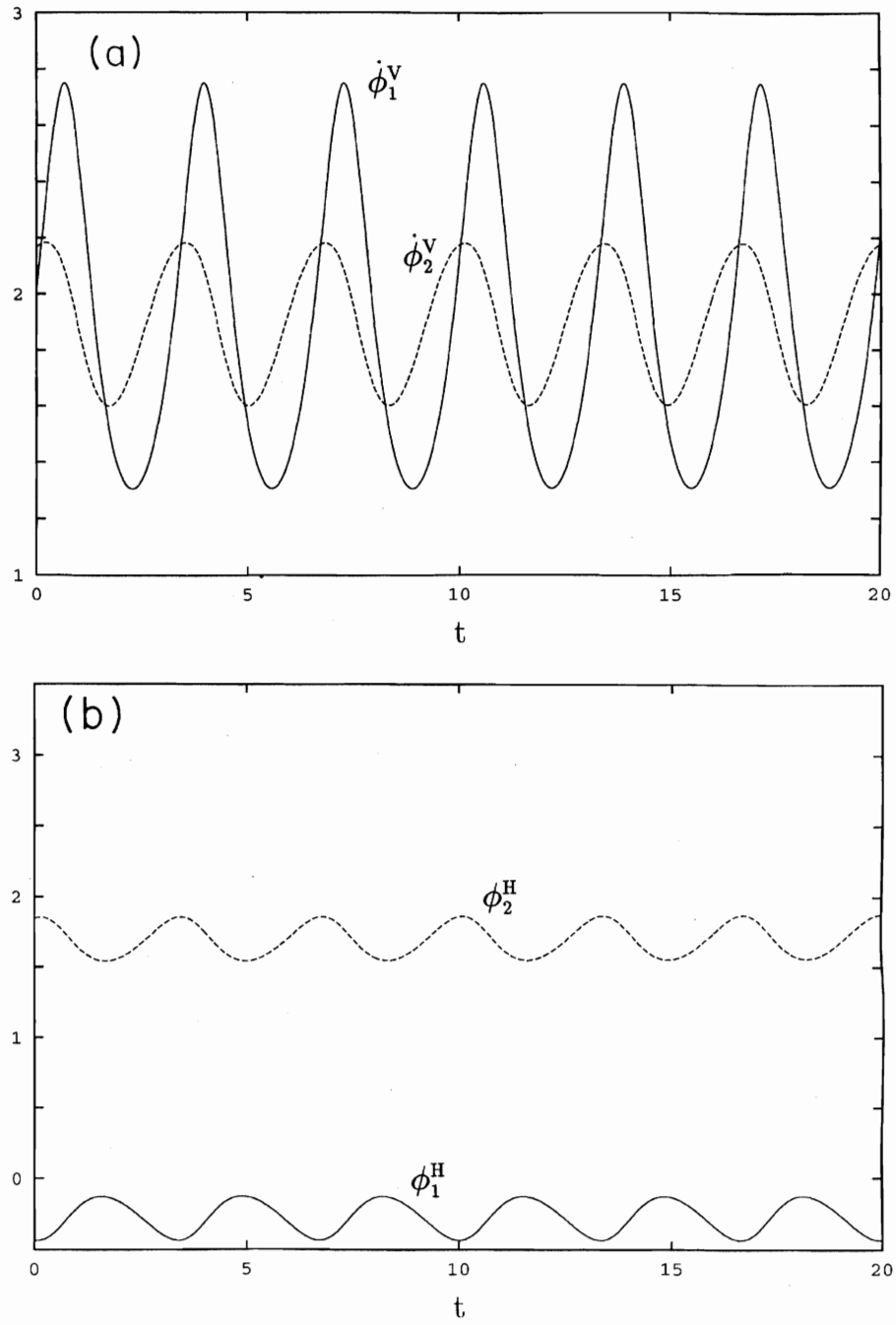

FIG. 4. Synchronized state of the plaquette: $I_{c_1}^V = 1.0$, $I_{c_2}^V = 0.4$, $I_{c_1}^H = 0.3$, $I_{c_2}^H = 0.08$, $I = 2.0$, and all resistances equal to unity. (a) The voltage oscillations of the vertical junctions $\dot{\phi}_1^V(t)$ and $\dot{\phi}_2^V(t)$ show frequency locking. (b) The phases $\phi_1^H(t)$ and $\phi_2^H(t)$ oscillate with zero average growth, signifying that no net regular current flows across the horizontal junctions. Note that the system is frequency locked despite high levels of disorder.

$$\left| \frac{(I_{c_1}^V)^2 - (I_{c_2}^V)^2}{4 I I_{c,\min}^H} \right| \leq 1, \tag{8}$$

where $I_{c,\min}^H \equiv \min(I_{c_1}^H, I_{c_2}^H)$.

Two features of this transition formula are worthy of note. First, it reveals that the plaquette can tolerate a surprisingly large amount of disorder before frequency locking is lost. (This is supported by numerical simulations; see Figs. 4 and 5.) Second, it suggests that deviations in the critical currents of the vertical junctions play a more crucial role than the deviations in the horizontal junctions, since a frequency-locked state is apparently possible whenever $I_{c_1}^V = I_{c_2}^V$, regardless of the status of the horizontal junctions. This feature generalizes to an arbitrary $(N \times M)$ array, as can be seen by the following argument. Suppose we keep the critical currents I_c for the vertical junctions in (2b) the same, but allow the critical currents for the horizontal junctions of the array

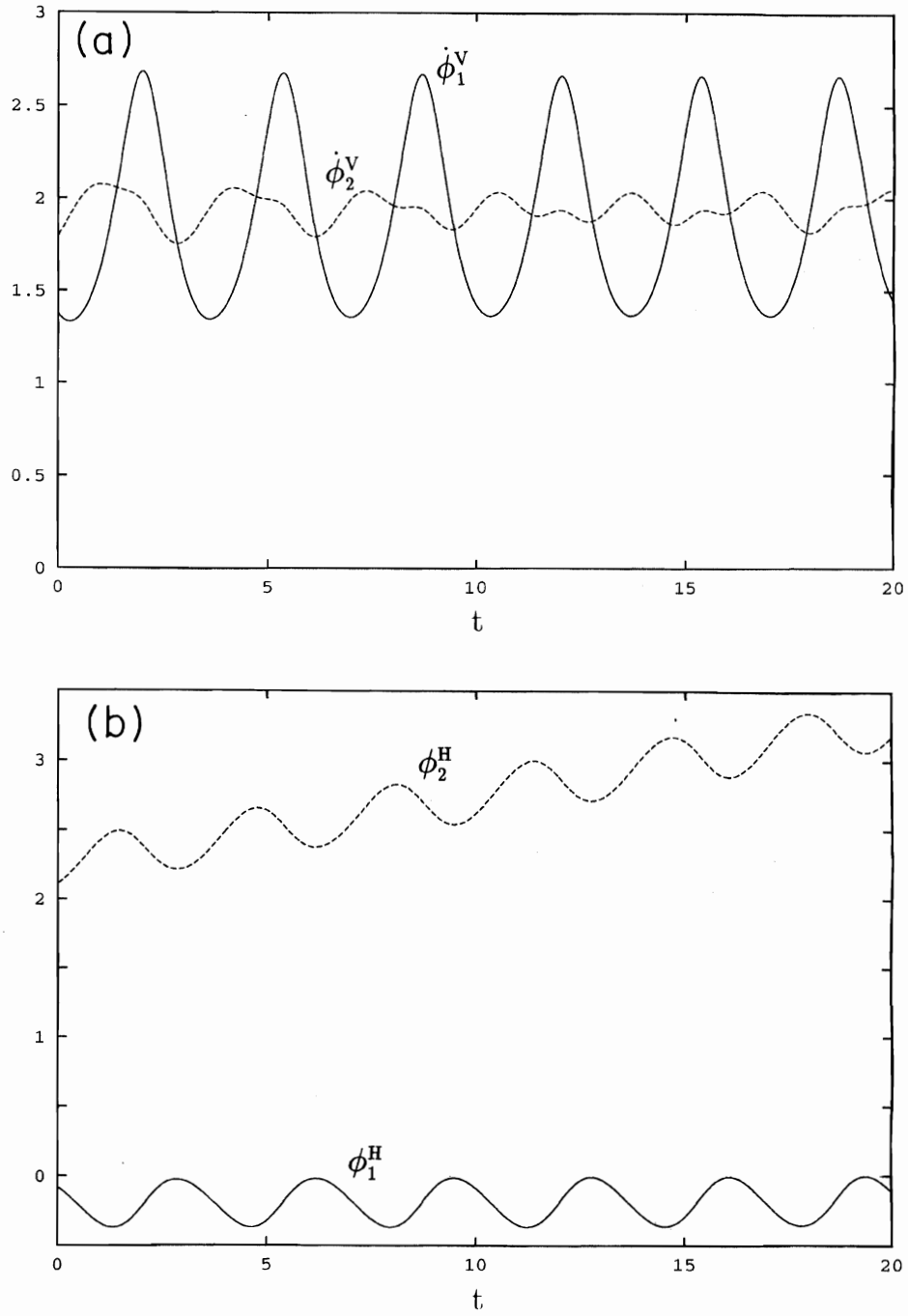

FIG. 5. Desynchronized state of the plaquette: $I_{c_1}^V = 1.0$, $I_{c_2}^V = 0.4$, $I_{c_1}^H = 0.3$, $I_{c_2}^H = 0.01$, $I = 2.0$, and all resistances equal to unity. (a) The voltage oscillations of the vertical junctions $\dot{\phi}_1^V(t)$ and $\dot{\phi}_2^V(t)$ are unlocked. (b) The horizontal phase $\phi_2^H(t)$ displays linear growth on average.

to be completely arbitrary [i.e., set $I_c \to I_{c_{ij}}^H$ in (2a)]. We then observe that there exists a frequency-locked solution of the form $\phi_{ij}^V = \phi^{\text{in}}(t+\delta_i), \phi_{ij}^H = 0$. Hence, disorder in the horizontal junctions does not by itself have any direct effect on the existence of a frequency-locked solution.

The arguments leading to transition criterion (8) can be repeated, this time keeping the critical currents identical and instead allowing the resistances of the individual junctions to differ ($r \to r_i^{H,V}$). The resulting locking criterion, approximated for the limit of large bias current I, is

$$\left| \left(\frac{r_1^V - r_2^V}{r_1^V + r_2^V} \right) \frac{I}{I_c} \right| \leq 1. \tag{9}$$

Observe that as I increases, the variation in the resistances of the vertical junctions must become correspondingly small if locking is to be maintained. This is simple to understand. For large I, most of the current passing through the vertical junctions is normal; the supercurrent, represented by the nonlinear terms in (5c) and (5d), becomes negligible, as does the cross-current $\triangle$. Consequently, the system (5c) and (5d) is

effectively linear, and the frequency of oscillation for the junctions ϕ_1^V and ϕ_2^V is proportional to $r_1^V I$ and $r_2^V I$, respectively. Thus, in order for the frequencies to be locked, we expect that the deviation $|r_1^V - r_2^V|$ must be relatively small, i.e., $O(1/I)$. We again see that variations in the horizontal junctions are less important than those of the vertical junctions. This property can be extended to the full $(N \times M)$ array by an argument similar to that given above.

B. Mathematical analysis of the plaquette

In this section we pursue more rigorously the preceding physical arguments with a more quantitative analysis. In particular, we demonstrate that frequency locking in the plaquette not only is possible, but that the system is dynamically driven to the frequency-locked state. That is, the frequency-locked state is an attractor when the disorder is not too large. We also determine precisely how "large" this disorder can be before locking is lost, leading to a refinement of the transition formulas (8) and (9) and a unified description which simultaneously incorporates the effects of variations in both the critical currents and resistances. The analysis is based on a multiple time scale expansion, ensuring that the resulting dynamical description has a well-defined asymptotic limit.

We begin by putting the governing equations (5a)–(5d) into a more useful form. First, the system is nondimensionalized by rescaling time and defining dimensionless quantities as follows:

$$T=\left(\frac{2erI}{\hbar}\right)t, \quad \rho_i^H=\frac{r_i^H}{r}, \quad \rho_i^V=\frac{r_i^V}{r}, \quad \iota_i^H=\frac{I_{c_i}^H}{I}, \quad \iota_i^V=\frac{I_{c_i}^V}{I}, \tag{10}$$

where r denotes the average value of the (four) junction resistances. Note that by definition $\rho_1^H+\rho_2^H+\rho_1^V+\rho_2^V=4$. Next we introduce new phase variables

$$\phi_D^V=\frac{\phi_1^V-\phi_2^V}{2}, \quad \phi_A^V=\frac{\phi_1^V+\phi_2^V}{2}. \tag{11}$$

ϕ_D^V measures the difference between the two vertical junction variables, and ϕ_A^V their average. This is useful since *any solution $\phi_D^V(T)$ which remains bounded in time corresponds to a frequency-locked state of the plaquette.* The governing equations are

$$\partial_T \phi_D^V=\frac{1}{2}[(\rho_1^V-\rho_2^V)-(\rho_1^V+\rho_2^V)\tilde{\triangle}-\iota_1^V\rho_1^V\sin(\phi_A^V+\phi_D^V) + \iota_2^V\rho_2^V\sin(\phi_A^V-\phi_D^V)], \tag{12a}$$

$$\partial_T \phi_A^V=\frac{1}{2}[(\rho_1^V+\rho_2^V)-(\rho_1^V-\rho_2^V)\tilde{\triangle}-\iota_1^V\rho_1^V\sin(\phi_A^V+\phi_D^V) - \iota_2^V\rho_2^V\sin(\phi_A^V-\phi_D^V)], \tag{12b}$$

$$\partial_T \phi_1^H=\rho_1^H\tilde{\triangle}-\iota_1^H\rho_1^H\sin(\phi_1^H), \tag{12c}$$

where the dimensionless cross current is given by

$$\tilde{\triangle}=\frac{1}{4}[(\rho_1^V-\rho_2^V)+\iota_1^H\rho_1^H\sin(\phi_1^H)+\iota_2^V\rho_2^V\sin(\phi_A^V-\phi_D^V) - \iota_1^V\rho_1^V\sin(\phi_A^V+\phi_D^V)-\iota_2^H\rho_2^H\sin(\phi_1^H-2\phi_D^V)]. \tag{13}$$

Note that in going from (5a)–(5d) to (12a)–(12c) and (13), we have used the constraint (6) to eliminate ϕ_2^H as a dynamical variable, and to rewrite the cross current in terms of the remaining variables.

Our formal calculation will concentrate on the high bias current regime ($I \gg I_c$), where the vertical junctions are overturning at high frequency. (In fact, our numerical simulations show that the resulting formula for the transition between locked and unlocked dynamics remains accurate well outside the high bias current limit.) Hence the quantities ι_1^V and ι_2^V appearing in (12a)–(12c) and (13) are small, and we therefore rewrite these explicitly as $\iota_1^V \to \epsilon\iota_1^V$, $\iota_2^V \to \epsilon\iota_2^V$, where ϵ represents a small parameter. Similarly, the quantities ι_1^H and ι_2^H will also be small, and we rescale them as follows: $\iota_1^H \to \epsilon^2\iota_1^H$, $\iota_2^H \to \epsilon^2\iota_2^H$. This difference in scaling between the horizontal and vertical junctions is motivated by the transition criterion (8), as can be seen by rewriting (8) in terms of the dimensionless currents defined in (10). It also is useful to reexpress the vertical resistances as $\rho_1^V \to \rho_1^{V,0}+\epsilon^2\rho_1^{V,2}$, $\rho_2^V \to \rho_2^{V,0}+\epsilon^2\rho_2^{V,2}$.

For a multiple time scale analysis,[17] we let $T_0 \equiv T$ denote the fast time scale in the problem, and introduce a slow time scale $T_1 \equiv \epsilon T$ and a superslow scale $T_2 \equiv \epsilon^2 T$. Thus,

$$\partial_T = \partial_{T_0}+\epsilon\partial_{T_1}+\epsilon^2\partial_{T_2}. \tag{14}$$

The dynamical variables, which are now assumed to depend on these three time scales, are expanded as follows:

$$\phi_D^V=\phi_D^{V,0}+\epsilon\phi_D^{V,1}+\epsilon^2\phi_D^{V,2}+\cdots, \tag{15a}$$

$$\phi_A^V=(\omega_0 T_0+\omega_2 T_2)+\phi_A^{V,0}+\epsilon\phi_A^{V,1}+\epsilon^2\phi_A^{V,2}+\cdots, \tag{15b}$$

$$\phi_1^H=\phi_1^{H,0}+\epsilon\phi_1^{H,1}+\epsilon^2\phi_1^{H,2}+\cdots. \tag{15c}$$

Note that in the expansion (15b) we have included a linear growth term $\omega_0 T_0+\omega_2 T_2$. This term, which is perhaps more transparent when rewritten as $(\omega_0+\epsilon^2\omega_2)T_0$, simply reflects the fact that ϕ_A^V, which measures the average phase of the vertical junctions, will overturn. The absence of a term $\epsilon\omega_1 T_1$ in the expansion is merely a matter of convenience — if included at the outset, it turns out to vanish at a later stage.

The basic procedure is as follows. The expansions (14) and (15a)–(15c) are substituted into the dynamical equations (12a)–(12c), and a hierarchy of equations is constructed based on powers of ϵ. At each order in the expansion, we obtain equations of the general form

$$\partial_{T_0}\phi=\cdots, \tag{16}$$

where $\phi=(\phi_D^V,\phi_A^V,\phi_1^H)$. The vector field appearing on the right-hand side of (16) will not depend on ϕ (to that order),

and can be naturally decomposed into two terms: a piece which oscillates on the fast time scale T_0 with zero mean, and a mean value piece which is constant on the fast time scale. In order for the asymptotic expansion (12a)–(12c) to remain valid over long time scales, each term in the expansion must remain bounded; otherwise its growth would destroy the assumed ordering in powers of ϵ. This requires that the mean value term on the right-hand side of (16) vanish. This requirement constitutes an additional constraint, known as a "solvability" or "nonresonance" condition. By requiring that it be satisfied the domain of validity of the asymptotic analysis is effectively extended. We now carry out this procedure.

At leading order in the expansion, we have

$$\partial_{T_0}\phi_D^{V,0}=\frac{1}{2}(\rho_1^{V,0}-\rho_2^{V,0})+\frac{1}{8}(\rho_1^{V,0}+\rho_2^{V,0})(\rho_1^{V,0}-\rho_2^{V,0}), \tag{17a}$$

$$\partial_{T_0}\phi_A^{V,0}=-\omega_0+\frac{1}{2}(\rho_1^{V,0}+\rho_2^{V,0})-\frac{1}{8}(\rho_1^{V,0}-\rho_2^{V,0})^2, \tag{17b}$$

$$\partial_{T_0}\phi_1^{H,0}=\frac{1}{4}\rho_1^{H,0}(\rho_1^{V,0}-\rho_2^{V,0}). \tag{17c}$$

The solvability condition for (17a) is that the right-hand side of this equation vanishes, so

$$\rho_1^{V,0}-\rho_2^{V,0}=0. \tag{18}$$

This condition has a simple physical interpretation: if the difference in the resistances of the two vertical junctions is too large, so that (18) is not satisfied, then the phase difference between the junctions will grow without bound [Eq. (17a)], and frequency locking will not be possible. This is consistent with our previous transition criterion (9). Next, the solvability condition associated with (17b) can be satisfied by choosing additionally

$$\omega_0=\frac{1}{2}(\rho_1^{V,0}+\rho_2^{V,0}). \tag{19}$$

The remaining solvability condition for (17c) is satisfied already by virtue of (18). Equations (17a)–(17c) may now be integrated, with the result

$$\phi_D^{V,0}=\phi_D^{V,0}(T_1,T_2),\quad \phi_A^{V,0}=\phi_A^{V,0}(T_1,T_2),$$

$$\phi_1^{H,0}=\phi_1^{H,0}(T_1,T_2), \tag{20}$$

where the notation (T_1,T_2) simply means that these quantities can evolve only on the slow time scales T_1 and T_2, being constant on the fast time scale T_0.

At next order in the expansion, the equations are

$$\partial_{T_0}\phi_D^{V,1}=-\partial_{T_1}\phi_D^{V,0}+\frac{1}{8}\iota_2^V\rho_2^{V,0}(4-\rho_1^{V,0}-\rho_2^{V,0})\sin(\omega_0T_0+\phi_A^{V,0}-\phi_D^{V,0})-\frac{1}{8}\iota_1^V\rho_1^{V,0}(4-\rho_1^{V,0}-\rho_2^{V,0})\sin(\omega_0T_0+\phi_A^{V,0}+\phi_D^{V,0}), \tag{21a}$$

$$\partial_{T_0}\phi_A^{V,1}=-\partial_{T_1}\phi_A^{V,0}-\frac{1}{2}\iota_2^V\rho_2^{V,0}\sin(\omega_0T_0+\phi_A^{V,0}-\phi_D^{V,0})-\frac{1}{2}\iota_1^V\rho_1^{V,0}\sin(\omega_0T_0+\phi_A^{V,0}+\phi_D^{V,0}), \tag{21b}$$

$$\partial_{T_0}\phi_1^{H,1}=-\partial_{T_1}\phi_1^{H,0}+\frac{1}{4}\iota_2^V\rho_2^{V,0}\rho_1^H\sin(\omega_0T_0+\phi_A^{V,0}-\phi_D^{V,0})-\frac{1}{4}\iota_1^V\rho_1^{V,0}\rho_1^H\sin(\omega_0T_0+\phi_A^{V,0}+\phi_D^{V,0}). \tag{21c}$$

The nonresonance conditions for these equations are very simple:

$$\partial_{T_1}\phi_D^{V,0}=0,\quad \partial_{T_1}\phi_A^{V,0}=0,\quad \partial_{T_1}\phi_1^{H,0}=0, \tag{22}$$

respectively. In view of (20) these imply $\phi_D^{V,0}=\phi_D^{V,0}(T_2)$, $\phi_A^{V,0}=\phi_A^{V,0}(T_2)$, and $\phi_1^{H,0}=\phi_1^{H,0}(T_2)$, revealing that these phase variables evolve only on the superslow time scale T_2. Equations (21a)–(21c) may now be integrated. We find

$$\phi_D^{V,1}=\frac{1}{8\omega_0}\iota_2^V\rho_2^{V,0}(-4+\rho_1^{V,0}+\rho_2^{V,0})\cos(\omega_0T_0+\phi_A^{V,0}-\phi_D^{V,0})-\frac{1}{8\omega_0}\iota_1^V\rho_1^{V,0}(-4+\rho_1^{V,0}+\rho_2^{V,0})\times\cos(\omega_0T_0+\phi_A^{V,0}+\phi_D^{V,0}), \tag{23a}$$

$$\phi_A^{V,1}=\frac{1}{2\omega_0}\iota_2^V\rho_2^{V,0}\cos(\omega_0T_0+\phi_A^{V,0}-\phi_D^{V,0})+\frac{1}{2\omega_0}\iota_1^V\rho_1^{V,0}\cos(\omega_0T_0+\phi_A^{V,0}+\phi_D^{V,0}), \tag{23b}$$

$$\phi_1^{H,1}=-\frac{1}{4\omega_0}\iota_2^V\rho_2^{V,0}\rho_1^H\cos(\omega_0T_0+\phi_A^{V,0}-\phi_D^{V,0})+\frac{1}{4\omega_0}\iota_1^V\rho_1^{V,0}\rho_1^H\cos(\omega_0T_0+\phi_A^{V,0}+\phi_D^{V,0}). \tag{23c}$$

Finally, the equations at $O(\epsilon^2)$ are constructed. We do not write these out explicitly, but instead focus on the resulting solvability conditions which describe the evolution of the three phases $\phi_D^{V,0}$, $\phi_A^{V,0}$, and $\phi_1^{H,0}$ on the superslow time scale. Only the first and third of these are relevant for our purposes, and after some algebra we find

$$\partial_{T_2}\phi_D^{V,0}=\frac{1}{8}(\rho_1^{V,2}-\rho_2^{V,2})(4-\rho_1^{V,0}-\rho_2^{V,0})+\frac{1}{128\omega_0}(8-\rho_1^{V,0}-\rho_2^{V,0})(4-\rho_1^{V,0}-\rho_2^{V,0})[(\iota_2^V\rho_2^{V,0})^2-(\iota_1^V\rho_1^{V,0})^2]$$

$$-\frac{1}{8}\iota_1^H\rho_1^H(\rho_1^{V,0}+\rho_2^{V,0})\sin(\phi_1^{H,0})+\frac{1}{8}\iota_2^H\rho_2^H(\rho_1^{V,0}+\rho_2^{V,0})\sin(\phi_1^{H,0}-2\phi_D^{V,0}), \tag{24a}$$

$$\partial_{T_2}\phi_1^{H,0}=\frac{1}{4}\rho_1^H(\rho_1^{V,2}-\rho_2^{V,2})+\frac{1}{64\omega_0}\rho_1^H(8-\rho_1^{V,0}-\rho_2^{V,0})[(\iota_2^V\rho_2^{V,0})^2-(\iota_1^V\rho_1^{V,0})^2]+\frac{1}{4}\iota_1^H\rho_1^H(\rho_1^H-4)\sin(\phi_1^{H,0})$$

$$-\frac{1}{4}\iota_2^H\rho_2^H\rho_1^H\sin(\phi_1^{H,0}-2\phi_D^{V,0}). \tag{24b}$$

Recall that the vertical junctions will be phase locked provided that $\phi_D^{V,0}$ remains bounded. Hence, the transition between locked and unlocked behavior in the plaquette [cf. (8) and (9)] is directly linked with the disappearance of stable, bounded solutions of (24a), (24b).

Equations (24a) and (24b) are readily analyzed. Note that they are of the form

$$\dot{\phi}_D^{V,0}=a_1+b_1\sin(\phi_1^{H,0})+c_1\sin(\phi_1^{H,0}-2\phi_D^{V,0}), \tag{25a}$$

$$\dot{\phi}_1^{H,0}=a_2+b_2\sin(\phi_1^{H,0})+c_2\sin(\phi_1^{H,0}-2\phi_D^{V,0}), \tag{25b}$$

where a_j, b_j, and c_j are constants. Generically, this system has either zero or four fixed points: a sink, a source, and two

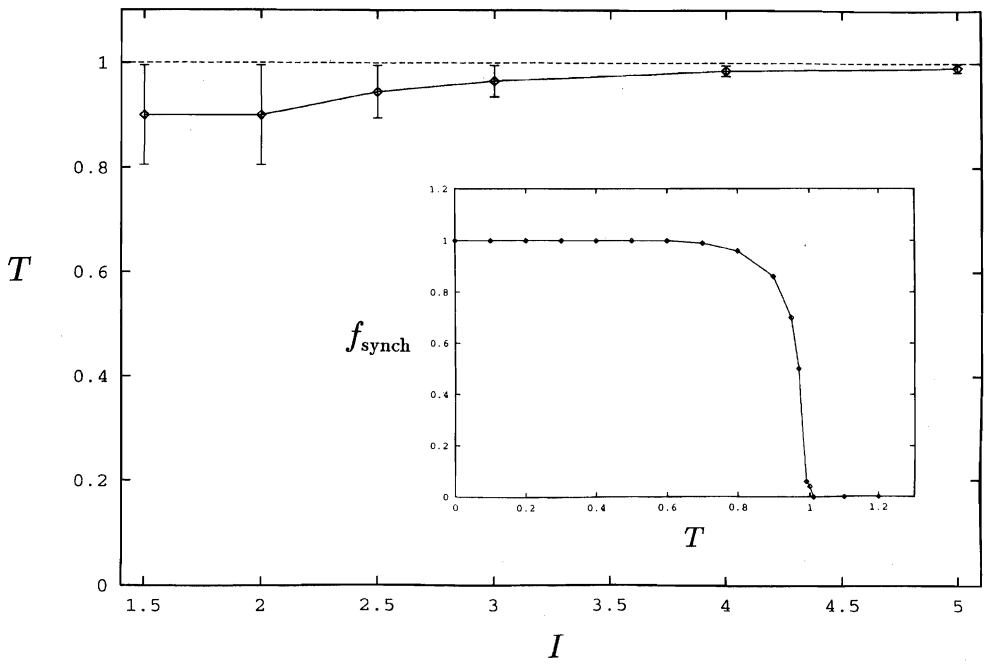

FIG. 6. Transition boundary between frequency-locked and unlocked states. The quantity T denotes the left-hand side of the transition formula (27). The dashed horizontal line at $T=1.0$ defines the theoretical threshold; the solid curve is the result of numerical simulations, and was constructed as follows. For a given value of T and bias current I (and $I_{c_1}^V$, r_1^V held fixed at 1.0), the critical currents $I_{c_2}^V$, $I_{c_1}^H$, and $I_{c_2}^H$ were randomly chosen in the interval (0.01,1.0), and the resistances r_2^V, r_1^H, and r_2^H randomly chosen between (0.9,1.0). A statistical sampling (based on 100 realizations of the disorder at each T,I) shows that below (above) the numerically determined curve, most states ($\geqslant 95\%$) are synchronized (unsynchronized). Within the transition regime around the curve (as defined by the error bars), states of both types were found. The inset shows the fraction of states which are synchronized (f_{synch}) as a function of T based on the sampling data at $I=1.5$; note the sharp transition to a desynchronized state near the predicted threshold. The theoretical prediction (27) remains surprisingly good even for low bias currents I, and gains in accuracy as the bias current is increased, as expected.

saddles. The sink corresponds to a stable, frequency-locked state. As the system parameters are varied, these four fixed points will simultaneously disappear in a double saddle-node bifurcation. This bifurcation thus defines the boundary between locked and unlocked behavior, and occurs at

$$\max\left[\left|\frac{a_1b_2-a_2b_1}{b_1c_2-b_2c_1}\right|,\quad \left|\frac{a_1c_2-a_2c_1}{b_1c_2-b_2c_1}\right|\right]=1. \tag{26}$$

[The four fixed points exist when the left-hand side of (26) is less than unity.] Using (24a), (24b), and (10), the locking criterion (26) may be reexpressed in terms of the original system parameters as

$$\left|\left(\frac{r_1^V-r_2^V}{r_1^V+r_2^V}\right)\frac{I}{I^H_{c,\min}} + \left(\frac{(r_2^VI^V_{c_2})^2-(r_1^VI^V_{c_1})^2}{2(r_1^V+r_2^V)^2II^H_{c,\min}}\right)\left(1+\frac{r_1^H+r_2^H}{r_1^V+r_2^V+r_1^H+r_2^H}\right)\right|\leq 1, \tag{27}$$

where, as before, $I^H_{c,\min}=\min(I^H_{c_1}, I^H_{c_2})$.

C. Discussion

The generalized transition formula (27) is the main result of this section. It quantifies the maximum amount of disorder which can be tolerated before frequency locking is lost. When the resistances of the junctions are all identical but the critical currents vary, it reduces to

$$\left|\frac{3}{16}\frac{(I^V_{c_2})^2-(I^V_{c_1})^2}{II^H_{c,\min}}\right|\leq 1, \tag{28}$$

which differs from our earlier approximation (8) only by a constant factor. Similarly, when the resistances vary but the critical currents are identical, we recover the previous result (9) (for $I\gg I_c$). We can now ascertain the relative importance of these two types of disorder. In particular, note that the transition criterion (27) is formally valid in the high bias current regime $I\gg I_c$. In this regime, the plaquette is much more sensitive to the size of the deviations in the resistances of the (vertical) junctions than to deviations in the critical currents. Synchronization will only be possible if the deviation in resistances is sufficiently small, i.e., $|r_1^V-r_2^V|\sim O(I_c/I)$. In this case, the critical currents of the junctions play only a minor role. If, however, the deviation in the resistances is reduced further [to $O(I_c^2/I^2)$], and the critical currents of the horizontal junctions are small [$O(I_c/I)$], then the variations in both the resistances and critical currents will contribute significantly.

This distinction, however, between the effects of variations in the resistances and critical currents in different regimes is somewhat artificial, in part because the transition criterion (27) remains quite accurate well outside the high bias current limit, and in part because the two types of disorder are dynamically linked and cannot be fully separated, as is clear from (27). The essential point is that *both types of disorder can potentially be important in terms of the dynamical behavior of the system, and that this can be true even if the deviation in the resistances is small compared to that of the critical currents.* Lastly, we note from (27) that in the absence of variations in the vertical junctions, variations in the horizontal junction characteristics do not directly effect the synchronization properties of the system and it always remains locked. However, when variations in the vertical junctions are also present, the variations in the horizontal junctions will effect the synchronization. In Fig. 6 we map out the boundary between the locked and unlocked regions, and compare the analytic prediction with numerical simulations of the disordered plaquette. The agreement is quite good.

The multiple time scale anaylsis not only allows us to refine and generalize the transition criteria (8) and (9), but lets us construct a general understanding of the effects of disorder. In particular, imagine starting with identical junctions and then slowly introduce disorder. For identical junctions, there exists a stable fixed point at the origin in the reduced system (24a) and (24b), which corresponds to the in-phase state. As disorder is added, this fixed point shifts slightly: physically, this corresponds to a small phase shift developing between the two vertical junctions. (This phase shift is not truly constant in time owing to small oscillatory terms of order ϵ in the expansion.) The vertical junctions are therefore frequency locked, and also approximately phase locked, and the horizontal junctions are weakly activated. As the disorder is increased, the fixed point migrates further from the origin until finally, for sufficiently large disorder, it disappears in a saddle-node bifurcation and frequency locking is lost. It is simple to show that at the bifurcation point [see (26), (25a), and (25b)]

$$\sin(\phi_1^{H,0})=\pm 1 \quad \text{or} \quad \sin(\phi_1^{H,0}-2\phi_D^{V,0})=\pm 1. \tag{29}$$

Note that $\phi_1^{H,0}-2\phi_D^{V,0}$ is by definition (6) and (11) just the phase difference across the second horizontal junction of the system, $\phi_2^{H,0}$. Hence we see that *frequency locking is lost when the supercurrent shunted by either horizontal junction reaches its maximum possible value.* This statement is only approximate owing to small oscillatory correction terms in the asymptotic expansion, but is consistent with, and in fact justifies, the physical argument of Sec. III A.

IV. DYNAMICS BETWEEN ROWS

Recall that for ideal $N\times M$ arrays there exists a neutral stability between rows for the in-phase state: the junctions are phase locked within each row, but merely frequency locked from one row to the next. It is not clear *a priori* what the effects of disorder might be, and a number of possibilities exist. For instance, the disorder might have little qualitative effect so that different rows remain frequency locked but not phase locked; or disorder might induce phase locking between rows;[3] or disorder might destroy frequency locking altogether.

In this section we show that disorder typically destroys frequency locking between the rows. We note that disorder has precisely this effect on one-dimensional arrays: e.g., for the case of two junctions (Fig. 7) the governing equations are

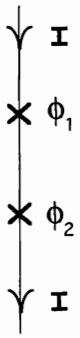

FIG. 7. A linear array consisting of two vertical junctions ϕ_1 and ϕ_2.

$$\frac{\hbar}{2er_1}\dot{\phi}_1+I_{c_1}\sin(\phi_1)=I, \tag{30a}$$

$$\frac{\hbar}{2er_2}\dot{\phi}_2+I_{c_2}\sin(\phi_2)=I, \tag{30b}$$

so that if the junction parameters are not identical the two junctions clearly oscillate with different frequencies. Unfortunately, this simple argument cannot be applied more generally because the junctions in (30a) and (30b) are fundamentally uncoupled, unlike what occurs in general 2D arrays. We therefore consider disorder in the simplest 2D array which allows for dynamical coupling between junctions in different rows.

A. The double plaquette

The "double plaquette" is depicted in Fig. 8. From (2a), (3), and (4), the governing equations may be written as

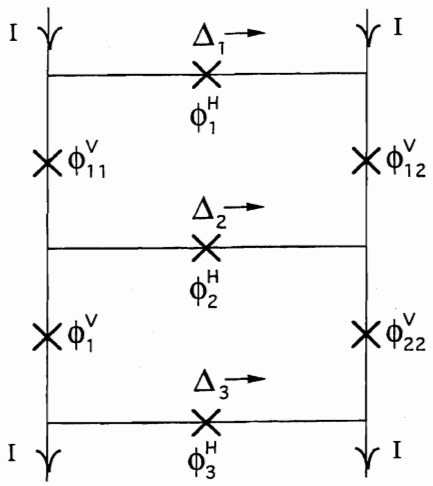

FIG. 8. The double plaquette. The vertical junctions in the first row are denoted by ϕ_{11}^V and ϕ_{12}^V, and those in the second by ϕ_{21}^V and ϕ_{22}^V. The horizontal junctions are ϕ_1^H, ϕ_2^H, and ϕ_3^H. Δ_1, Δ_2, and Δ_3 represent the induced currents shunted across the horizontal junctions.

$$\frac{\hbar}{2er_1^H}\dot{\phi}_1^H+I_{c_1}^H\sin(\phi_1^H)=\Delta_1, \tag{31a}$$

$$\frac{\hbar}{2er_2^H}\dot{\phi}_2^H+I_{c_2}^H\sin(\phi_2^H)=\Delta_2, \tag{31b}$$

$$\frac{\hbar}{2er_3^H}\dot{\phi}_3^H+I_{c_3}^H\sin(\phi_3^H)=\Delta_3, \tag{31c}$$

$$\frac{\hbar}{2er_{11}^V}\dot{\phi}_{11}^V+I_{c_{11}}^V\sin(\phi_{11}^V)=I-\Delta_1, \tag{31d}$$

$$\frac{\hbar}{2er_{12}^V}\dot{\phi}_{12}^V+I_{c_{12}}^V\sin(\phi_{12}^V)=I+\Delta_1, \tag{31e}$$

$$\frac{\hbar}{2er_{21}^V}\dot{\phi}_{21}^V+I_{c_{21}}^V\sin(\phi_{21}^V)=I-\Delta_1-\Delta_2, \tag{31f}$$

$$\frac{\hbar}{2er_{22}^V}\dot{\phi}_{22}^V+I_{c_{22}}^V\sin(\phi_{22}^V)=I+\Delta_1+\Delta_2, \tag{31g}$$

along with constraint relations

$$\Delta_1+\Delta_2+\Delta_3=0, \tag{32a}$$

$$\phi_1^H+\phi_{12}^V-\phi_2^H-\phi_{11}^V=0, \tag{32b}$$

$$\phi_2^H+\phi_{22}^V-\phi_3^H-\phi_{21}^V=0. \tag{32c}$$

Here, Δ_1, Δ_2, and Δ_3 denote the total current across the three horizontal junctions, respectively, and we have allowed the junction critical currents and resistances to vary.

As before, we can analyze the effects of disorder in Eqs. (31a)–(31g) and (32a)–(32c) using a multiple time scale method. Before doing so, however, it is instructive to consider a special realization of disorder where we can instantly deduce its effect. Suppose that all vertical junctions lying in the same row are identical ($I_{c_{ij}}^V=I_{c_{ij'}}^V, r_{ij}^V=r_{ij'}^V$), but that they differ from one row to the next. Then, as is readily verified by inspection, Eqs. (31a)–(31g) and (32a)–(32c) admit a solution in which all horizontal junctions are inactive and where all vertical junctions lying in a given row oscillate exactly in phase at some frequency, but where this oscillation frequency is different for the two rows. Thus, disorder of this special type destroys frequency locking between rows. (Remarkably, though, it preserves the neutral stability.) A similar result holds for $N\times M$ arrays with this type of disorder.

B. Multiscale analysis

We now demonstrate the absence of frequency locking in the double plaquette for general disorder using a multiple scale expansion. In order to simplify the algebra we only

consider variations in the critical currents. The governing equations (31a)–(31g) and (32a)–(32c) can be put in a more useful form by defining

$$\phi^V_{D1}=\frac{\phi^V_{11}-\phi^V_{12}}{2},\quad \phi^V_{D2}=\frac{\phi^V_{21}-\phi^V_{22}}{2},\quad \phi^V_{A1}=\frac{\phi^V_{11}+\phi^V_{12}}{2},$$

$$\phi^V_{A2}=\frac{\phi^V_{21}+\phi^V_{22}}{2}, \tag{33}$$

and

$$\phi^H=\phi^H_1+\phi^H_2+\phi^H_3, \tag{34}$$

where ϕ^V_{D1} and ϕ^V_{D2} measure the phase difference between the two vertical-junction variables in the top row and bottom row, respectively; ϕ^V_{A1} and ϕ^V_{A2} measure the average phases for each row. Note that the two rows will be frequency locked if $\phi^V_{A1}-\phi^V_{A2}$ remains bounded. For convenience we set $\hbar/2er=1$. In these new variables, the system becomes

$$\dot\phi^V_{D1}=-\triangle_1-\frac{1}{2}I^V_{c_{11}}\sin(\phi^V_{A1}+\phi^V_{D1})+\frac{1}{2}I^V_{c_{12}}\sin(\phi^V_{A1}-\phi^V_{D1}), \tag{35a}$$

$$\dot\phi^V_{D2}=-\triangle_1-\triangle_2-\frac{1}{2}I^V_{c_{21}}\sin(\phi^V_{A2}+\phi^V_{D2})+\frac{1}{2}I^V_{c_{22}}\sin(\phi^V_{A2}-\phi^V_{D2}), \tag{35b}$$

$$\dot\phi^V_{A1}=I-\frac{1}{2}I^V_{c_{11}}\sin(\phi^V_{A1}+\phi^V_{D1})-\frac{1}{2}I^V_{c_{12}}\sin(\phi^V_{A1}-\phi^V_{D1}), \tag{35c}$$

$$\dot\phi^V_{A2}=I-\tfrac{1}{2}I^V_{c_{21}}\sin(\phi^V_{A2}+\phi^V_{D2})-\tfrac{1}{2}I^V_{c_{22}}\sin(\phi^V_{A2}-\phi^V_{D2}), \tag{35d}$$

$$\dot\phi^H=-I^H_{c_1}\sin\left(\frac{\phi^H+2\phi^V_{D2}+4\phi^V_{D1}}{3}\right)-I^H_{c_2}\sin\left(\frac{\phi^H+2\phi^V_{D2}-2\phi^V_{D1}}{3}\right)-I^H_{c_3}\sin\left(\frac{\phi^H-4\phi^V_{D2}-2\phi^V_{D1}}{3}\right), \tag{35e}$$

where

$$\triangle_1=-\frac{4}{15}I^V_{c_{11}}\sin(\phi^V_{A1}+\phi^V_{D1})+\frac{4}{15}I^V_{c_{12}}\sin(\phi^V_{A1}-\phi^V_{D1})-\frac{1}{15}I^V_{c_{21}}\sin(\phi^V_{A2}+\phi^V_{D2})+\frac{1}{15}I^V_{c_{22}}\sin(\phi^V_{A2}-\phi^V_{D2})$$
$$+\frac{4}{15}I^H_{c_1}\sin\left(\frac{\phi^H+2\phi^V_{D2}+4\phi^V_{D1}}{3}\right)-\frac{1}{15}I^H_{c_2}\sin\left(\frac{\phi^H+2\phi^V_{D2}-2\phi^V_{D1}}{3}\right)-\frac{1}{15}I^H_{c_3}\sin\left(\frac{\phi^H-4\phi^V_{D2}-2\phi^V_{D1}}{3}\right), \tag{36a}$$

$$\triangle_2=+\frac{1}{5}I^V_{c_{11}}\sin(\phi^V_{A1}+\phi^V_{D1})-\frac{1}{5}I^V_{c_{12}}\sin(\phi^V_{A1}-\phi^V_{D1})-\frac{1}{5}I^V_{c_{21}}\sin(\phi^V_{A2}+\phi^V_{D2})+\frac{1}{5}I^V_{c_{22}}\sin(\phi^V_{A2}-\phi^V_{D2})$$
$$-\frac{1}{5}I^H_{c_1}\sin\left(\frac{\phi^H+2\phi^V_{D2}+4\phi^V_{D1}}{3}\right)+\frac{2}{5}I^H_{c_2}\sin\left(\frac{\phi^H+2\phi^V_{D2}-2\phi^V_{D1}}{3}\right)-\frac{1}{5}I^H_{c_3}\sin\left(\frac{\phi^H-4\phi^V_{D2}-2\phi^V_{D1}}{3}\right). \tag{36b}$$

Introducing ϵ as a small parameter, we scale the critical currents $I^V_{c_{ij}}, I^H_{c_i}\to\epsilon I^V_{c_{ij}}, \epsilon I^H_{c_i}$, corresponding to the high bias current regime. Setting $\partial_t=\partial_{T_0}+\epsilon\partial_{T_1}+\partial_{T_2}$, the phases are then expanded as follows:

$$\phi^V_{D1}=\phi^{V,0}_{D1}+\epsilon\phi^{V,1}_{D1}+\epsilon^2\phi^{V,2}_{D1}, \tag{37a}$$

$$\phi^V_{D2}=\phi^{V,0}_{D2}+\epsilon\phi^{V,1}_{D2}+\epsilon^2\phi^{V,2}_{D2}, \tag{37b}$$

$$\phi^V_{A1}=(\omega_{1,0}T_0+\omega_{1,2}T_2)+\phi^{V,0}_{A1}+\epsilon\phi^{V,1}_{A1}+\epsilon^2\phi^{V,2}_{A1}, \tag{37c}$$

$$\phi^V_{A2}=(\omega_{2,0}T_0+\omega_{2,2}T_2)+\phi^{V,0}_{A2}+\epsilon\phi^{V,1}_{A2}+\epsilon^2\phi^{V,2}_{A2}, \tag{37d}$$

$$\phi^H=\phi^{H,0}+\epsilon\phi^{H,1}+\epsilon\phi^{H,2}. \tag{37e}$$

Substitution of these expansions leads to a hierarchy of equations. To lowest order we conclude that the phases $\phi^{V,0}_{D1}$, $\phi^{V,0}_{D2}$, $\phi^{V,0}_{A1}$, ϕ^V_{A2}, and $\phi^{H,0}$ depend solely on the slow time scales T_1 and T_2, and that the average rate of overturning for the vertical oscillators in each of the two rows is simply $\omega_{1,0}=\omega_{2,0}=I$. At $O(\epsilon)$, we find solvability conditions

$$\partial_{T_1}\phi_{D1}^{V,0} = -\frac{4}{15} I_{c_1}^{H} \sin\left(\frac{\phi^{H}+2\phi_{D2}^{V,0}+4\phi_{D1}^{V,0}}{3}\right) + \frac{1}{5} I_{c_2}^{H} \sin\left(\frac{\phi^{H}+2\phi_{D2}^{V,0}-2\phi_{D1}^{V,0}}{3}\right) + \frac{1}{15} I_{c_3}^{H} \sin\left(\frac{\phi^{H}-4\phi_{D2}^{V,0}-2\phi_{D1}^{V,0}}{3}\right), \quad (38a)$$

$$\partial_{T_1}\phi_{D2}^{V,0} = -\frac{1}{15} I_{c_1}^{H} \sin\left(\frac{\phi^{H}+2\phi_{D2}^{V,0}+4\phi_{D1}^{V,0}}{3}\right) - \frac{1}{5} I_{c_2}^{H} \sin\left(\frac{\phi^{H}+2\phi_{D2}^{V,0}-2\phi_{D1}^{V,0}}{3}\right) + \frac{4}{15} I_{c_3}^{H} \sin\left(\frac{\phi^{H}-4\phi_{D2}^{V,0}-2\phi_{D1}^{V,0}}{3}\right), \quad (38b)$$

$$\partial_{T_1}\phi^{H,0} = -I_{c_1}^{H} \sin\left(\frac{\phi^{H}+2\phi_{D2}^{V,0}+4\phi_{D1}^{V,0}}{3}\right) - I_{c_2}^{H} \sin\left(\frac{\phi^{H}+2\phi_{D2}^{V,0}-2\phi_{D1}^{V,0}}{3}\right) - I_{c_3}^{H} \sin\left(\frac{\phi^{H}-4\phi_{D2}^{V,0}-2\phi_{D1}^{V,0}}{3}\right), \quad (38c)$$

along with the trivial conditions $\partial_{T_1}\phi_{A1}^{V,0}=0$ and $\partial_{T_1}\phi_{A2}^{V,0}=0$. A key observation is that the origin of system (38a)–(38c) is an attractor for all values of the critical currents, as a simple linear stability calculation shows.

Finally, at $O(\epsilon^2)$, we obtain solvability conditions for $\phi_{A1}^{V,0}(T_2)$, and $\phi_{A2}^{V,0}(T_2)$. It is most instructive to rewrite these in terms of the difference between these two phases:

$$\partial_{T_2}(\phi_{A1}^{V,0}-\phi_{A2}^{V,0}) = (\omega_{2,2}-\omega_{1,2}) + \frac{11}{60I}\left[(I_{c_{21}}^{V})^2+(I_{c_{22}}^{V})^2 - (I_{c_{11}}^{V})^2-(I_{c_{12}}^{V})^2\right] - \frac{2}{15I} I_{c_{11}}^{V} I_{c_{12}}^{V} \cos(2\phi_{D1}^{V,0}) + \frac{2}{15I} I_{c_{21}}^{V} I_{c_{22}}^{V} \cos(2\phi_{D2}^{V,0}). \quad (39)$$

We know from (38a)–(38c) that $\phi_{D1}^{V,0}$ and $\phi_{D2}^{V,0}$ approach the origin on a "fast" time scale T_1 (i.e., fast compared to T_2), so we may replace these quantities by zero in Eq. (39). Since we require bounded solutions to (39), it follows that there will exist a frequency mismatch between the top and bottom rows of the double plaquette [see (37c) and (37d)], i.e.,

$$\omega_{1,2}-\omega_{2,2} = \frac{11}{60I}\left[(I_{c_{21}}^{V})^2+(I_{c_{22}}^{V})^2-(I_{c_{11}}^{V})^2-(I_{c_{12}}^{V})^2\right] - \frac{2}{15I} I_{c_{11}}^{V} I_{c_{12}}^{V} + \frac{2}{15I} I_{c_{21}}^{V} I_{c_{22}}^{V} \neq 0. \quad (40)$$

Hence we conclude that disorder destroys the frequency locking between rows, as claimed.

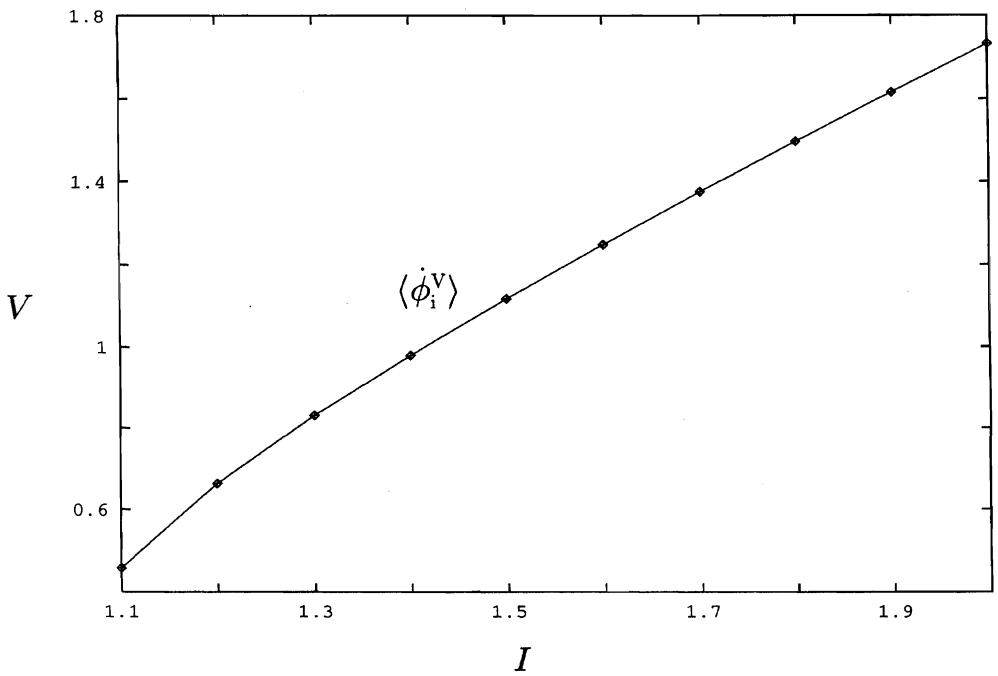

FIG. 9. *I-V* characteristic of an $N\times M$, *identical-junction* array in the in-phase state. The time-averaged voltage of the individual junctions $\{\langle\dot{\phi}_i^V\rangle\}$ is shown. In this state all vertical junctions ϕ_{ij}^V display the same *I-V* behavior; the horizontal junctions ϕ_{ij}^H are inactive. For different initial conditions (leading to states related to, but distinct from, the in-phase state), the same *I-V* behavior results.

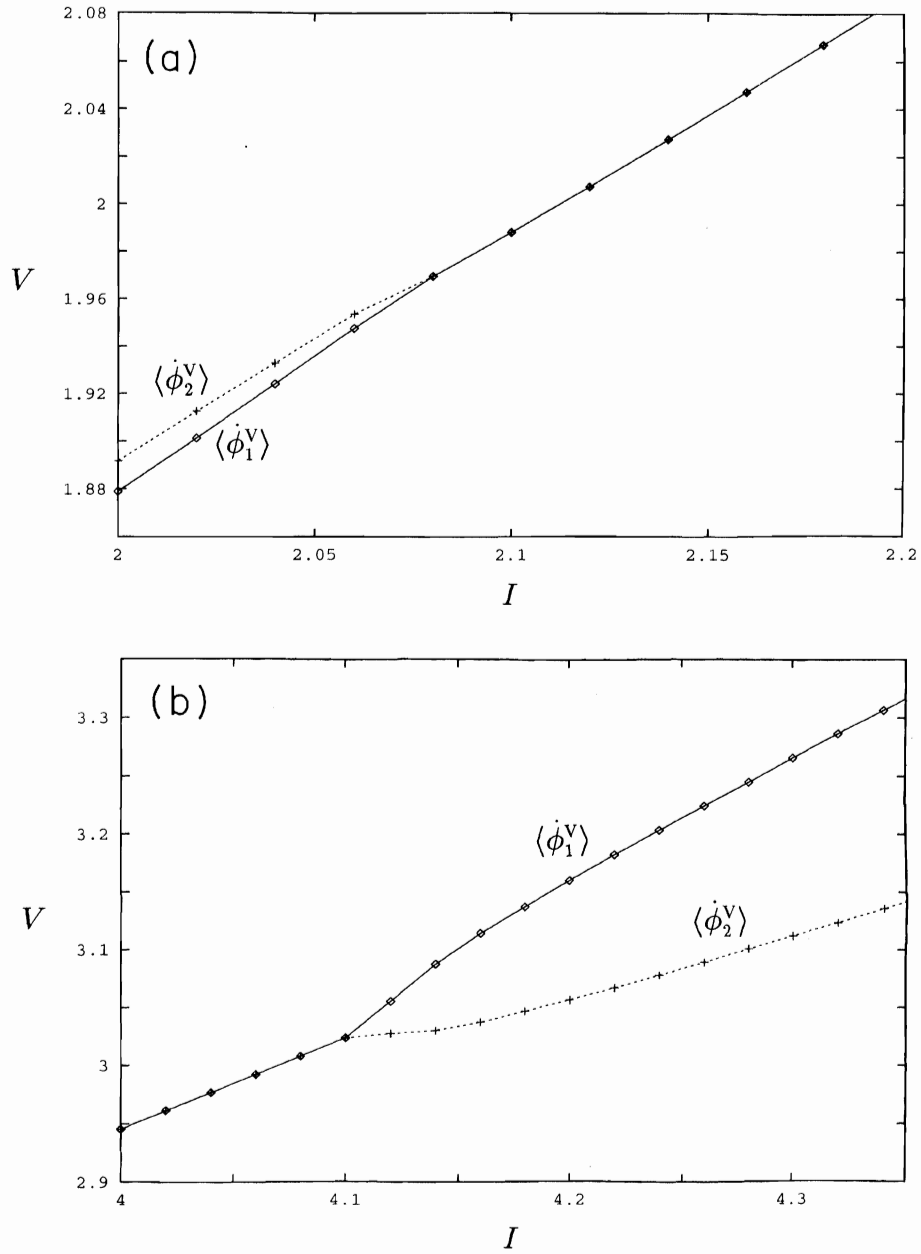

FIG. 10. *I-V* curve for the plaquette for large disorder. The time-averaged voltage across each junction $\langle\dot{\phi}_i^{H,V}\rangle$ is shown. (a) For critical currents $I_{c_1}^V=1.0$, $I_{c_2}^V=0.5$, $I_{c_1}^H=0.3$, $I_{c_2}^H=0.07$, and all resistances equal to unity. (b) For resistances $r_1^V=1.0$, $r_2^V=0.6$, $r_1^H=0.9$, $r_2^H=0.8$, and all critical currents equal to unity. Note the transition from synchronized to desynchronized behavior in each case; the observed transition values of the bias currents agree with the theoretical predictions [using (27)] to better than 5% and 2%, respectively.

V. DISCUSSION AND NUMERICAL SIMULATIONS

In this section we summarize our main results and present numerical simulations of various prototype 2D arrays. Figure 9 depicts the theoretical *I-V* curve for the in-phase state of an ideal $N\times M$ array with identical elements, showing the behavior of the junctions: all vertical junctions oscillate (i.e., overturn) at the same rate and in phase; the horizontal junctions remain inactive. Since this state is only neutrally stable, for different initial conditions the system will instead evolve to a state in which all vertical junctions *within a given row* oscillate in phase, but with overall phase shifts from one row to the next (the horizontal junctions remain inactive). In either case, the *I-V* characteristics for these states are the same, since the vertical junctions always oscillate with the same frequency (i.e., voltage). Nevertheless, because phase shifts can exist between different rows, there is a natural dichotomy between the behavior seen across a given row of the array and that found moving downwards from one row to the next. The neutral stability is associated with this downward direction.

This picture changes with the introduction of disorder, though a dichotomy between intrarow and inter-row behaviors persists. Our analytic results for the plaquette show that low or moderate levels of disorder destroy the in-phase, intrarow behavior, but nonetheless preserve (1:1) frequency locking between the vertical junctions within a row. The physical mechanism responsible for this frequency locking is the induced supercurrents shunted by the horizontal junc-

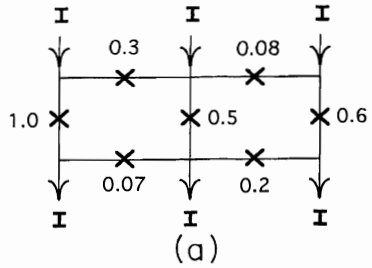

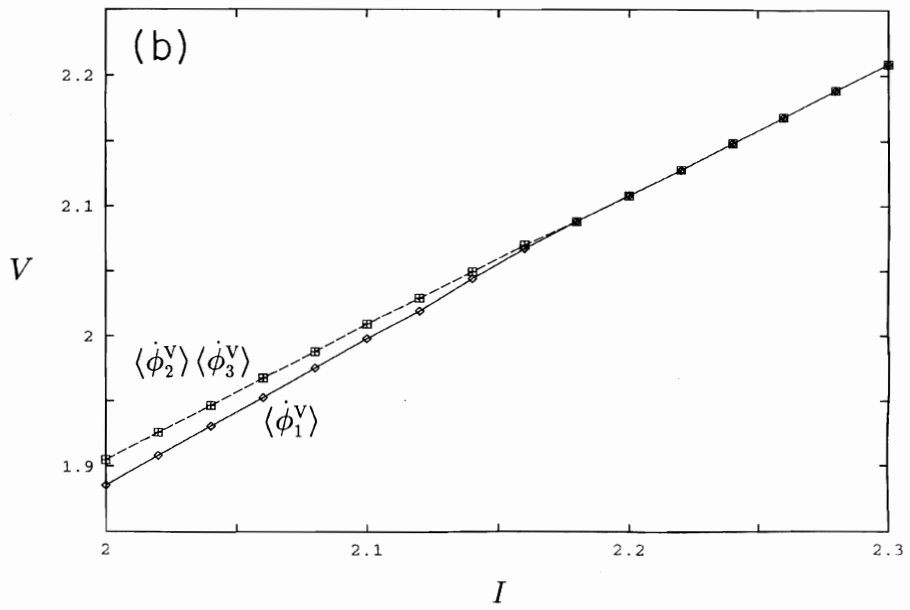

FIG. 11. (a) A row of junctions. The critical current of each junction is indicated (high disorder). (b) The corresponding I-V curves, showing a transition to a desynchronized state. The junction resistances are all equal to unity. After the transition, two of the vertical junctions continue to be frequency locked in this example. Note that for lower levels of disorder no fork in the I-V curve would exist.

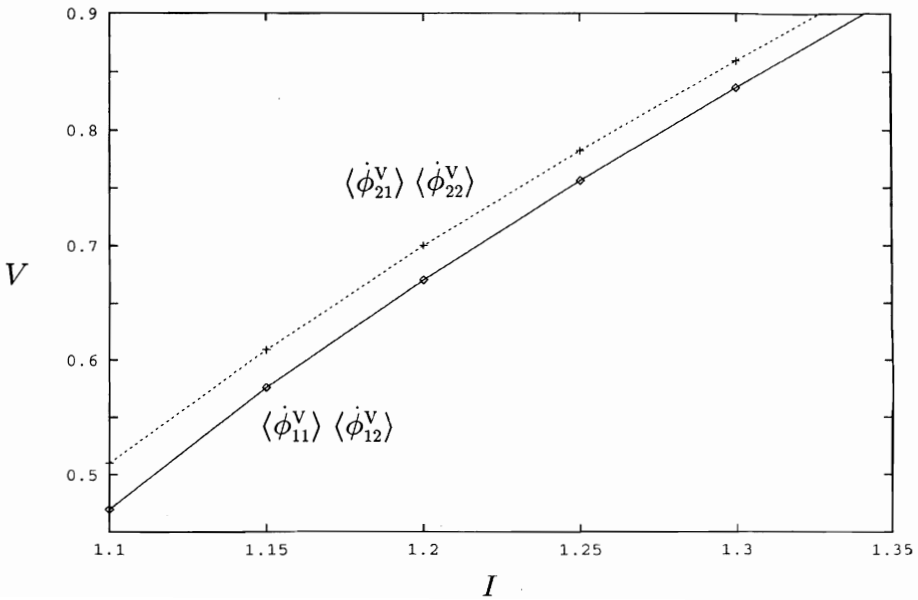

FIG. 12. I-V curves for the double plaquette with weak disorder ($I_{c_{11}}^V=1.00$, $I_{c_{12}}^V=0.99$, $I_{c_{21}}^V=0.98$, $I_{c_{22}}^V=0.97$, $I_{c_1}^H=0.99$, $I_{c_2}^H=0.97$, $I_{c_3}^H=0.98$). The vertical junctions in the same row are frequency locked, but the characteristic frequency of each row is different.

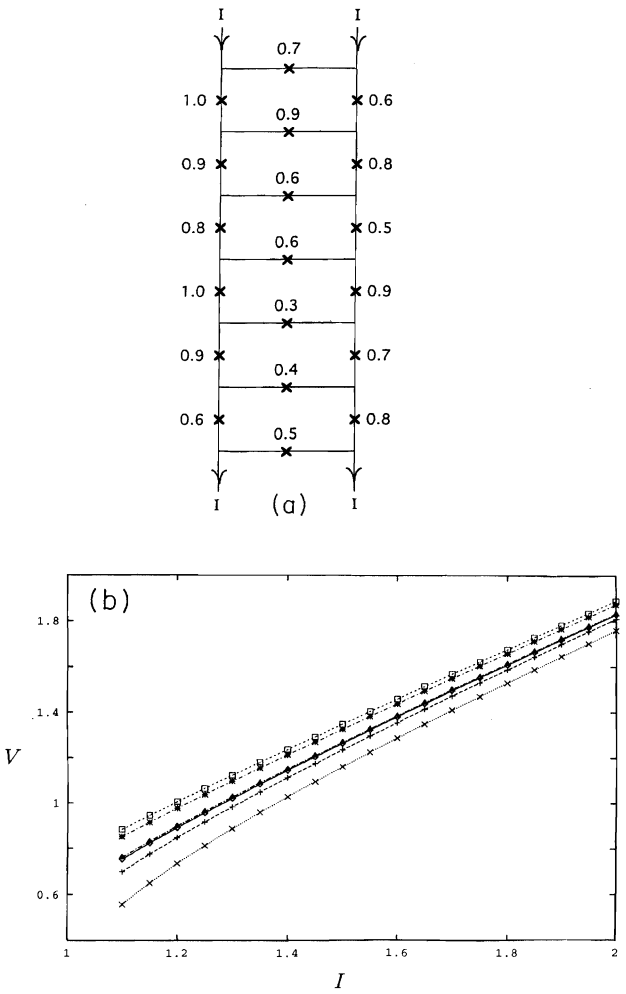

FIG. 13. (a) A 6×2 array. The critical current of each junction is indicated (moderate disorder). (b) *I-V* curves, demonstrating that the vertical junctions in the six rows have different oscillation frequencies (two of these frequencies are close in value and difficult to distinguish in the plot). Within each row, the vertical junctions are frequency locked. Intra-row locking would be destroyed at higher levels of disorder (not shown).

tions, which compensate for the inhomogeneities associated with the disorder. For high levels of disorder, this mechanism will fail when the required supercurrent exceeds the maximum allowable supercurrent which can be shunted by the horizontal junctions: frequency locking is lost when regular shunt currents begin to flow. This behavior is depicted in the *I-V* characteristics of the plaquette (Fig. 10). The separation of the *I-V* curves of the different vertical (or horizontal) junctions indicates that the transition from a frequency-locked to an unlocked state has occurred. We emphasize that this transition sets in only at high levels of disorder [as defined by transition criterion (27)]; at lower levels of disorder there is no transition, and the *I-V* characteristics closely resemble that of the idealized identical junction case (Fig. 9). We note also that the transition point is somewhat more sensitive to variations in the resistances than to variations in the critical currents, at least in the case of high bias current. If instead of an isolated plaquette we consider a series of plaquettes laid down horizontally alongside one another (forming a $2\times N$ array), then the intrarow frequency-locking mechanism identified in the single plaquette will continue to operate, promoting frequency locking of vertical junctions across the entire row (Fig. 11). As before, this is accomplished by means of induced supercurrents being shunted across the horizontal junctions, and a transition occurs at sufficiently high levels of disorder.

The primary effect of disorder on *inter*-row behavior is revealed by the (3×2) double plaquette described in Sec. IV. We showed that *arbitrarily small* amounts of disorder destroy the frequency locking between rows. A typical *I-V* plot for the double plaquette is shown in Fig. 12 for weak disorder. Observe that the vertical junctions in different rows are no longer frequency locked despite the very low level of disorder. The junctions within the same row continue to be locked via the mechanism described above (unless the disorder is so high that this intrarow locking itself breaks down). Our numerical simulations verify that these behaviors persist if additional plaquettes are laid down vertically beneath the double plaquette, forming an $N\times2$ array (Fig. 13).

In summary, based on these numerical simulations of larger arrays, we conclude that our theoretical analysis of two prototype systems—the plaquette and double plaquette —captures the two principal physical mechanisms at work in large disordered arrays of resistively shunted Josephson junctions, and provides us with (at least a partial) understanding of the dynamical behavior of these systems. In particular, the vertical junctions within each row maintain 1:1 frequency locking provided the disorder is not too large, but the different rows operate at different frequencies for arbitrarily small disorder.

ACKNOWLEDGMENTS

We gratefully acknowledge useful discussions with Sam Benz. This work was supported in part by the Office of Naval Research under Contract No. N00014-J-1257.

[1] A. Barone and G. Paternò, *Physics and Application of the Josephson Effect* (Wiley, New York, 1982).
[2] K. K. Likharev, *Dynamics of Josephson Junctions and Circuits* (Gordon and Breach, New York, 1986).
[3] K. Wiesenfeld, S.P. Benz, and P.A.A. Booi, J. Appl. Phys. **76**, 3835 (1994).
[4] P. Hadley and M.R. Beasley, Appl. Phys. Lett. **50**, 621 (1987).
[5] K. Wiesenfeld and P. Hadley, Phys. Rev. Lett. **62**, 1335 (1989).
[6] K.Y. Tsang, S.H. Strogatz, and K. Wiesenfeld, Phys. Rev. Lett. **66**, 1094 (1991).
[7] S. Nichols and K. Wiesenfeld, Phys. Rev. A **45**, 8430 (1992).
[8] S. Watanabe and S.H. Strogatz, Phys. Rev. Lett. **70**, 2391 (1993); Physica D **74**, 197 (1994).
[9] P.A.A. Booi and S.P. Benz, Appl. Phys. Lett. **64**, 2163 (1994).

[10] P. Hadley, Ph.D. dissertation, Stanford University, 1989.
[11] R.L. Kautz, IEEE Trans. Appl. Supercond. **5**, 2702 (1995).
[12] M. Darula, P. Seidel, F. Busse, and Š. Beňačka, Supercond. Sci. Technol. **7**, 317 (1994).
[13] M. Octavio, C.B. Whan, and C.J. Lobb, Appl. Phys. Lett. **60**, 766 (1992).
[14] S.P. Benz and C.J. Burroughs, Appl. Phys. Lett. **58**, 2162 (1991).
[15] G. Filatrella and K. Wiesenfeld, J. Appl. Phys. **78**, 1878 (1995).
[16] B.H. Larsen and S.P. Benz, Appl. Phys. Lett. (to be published).
[17] D.W. Jordan and P. Smith, *Nonlinear Ordinary Differential Equations* (Clarendon Press, Oxford, 1987).